Reactivity of chromophoric dissolved organic matter (CDOM) to sulfate radicals: Reaction kinetics and structural transformation

Suona Zhang, Valentin Rougé, Leonardo Gutierrez, Jean-Philippe Croué

Reactivity of chromophoric dissolved organic matter (CDOM) to sulfate radicals: Reaction kinetics and structural transformation

Suona Zhang [a], Valentin Rouge [a], Leonardo Gutierrez [b,c] , Jean-Philippe Croue [a,c] *

[a] Curtin Water Quality Research Centre, Department of Chemistry, Curtin University, Australia
[b] Facultad del Mar y Medio Ambiente, Universidad del Pacifico, Ecuador
[c] Institut de Chimie des Milieux et des Materiaux IC2MP UMR 7285 CNRS, Universite de Poitiers, France

* Corresponding author: Tel.: +61 (0) 8 9266 9793
E-mail address: jean.philippe.croue@univ-poitiers.fr

Abstract

Sulfate radical ($SO_4^{\bullet-}$) has been extensively studied as a promising alternative in advanced oxidation processes (AOPs) for water treatment. However, little is known about its reactivity to the ubiquitous dissolved organic matter (DOM) in water bodies. $SO_4^{\bullet-}$ would selectively react with electron rich moieties in DOM, known as chromophoric DOM (CDOM), due to its light absorbing property. In this study, the reactivity and typical structural transformation of CDOM with $SO_4^{\bullet-}$ was investigated. Four well characterized hydrophobic DOM fractions extracted from different surface water sources were selected as model CDOM. $SO_4^{\bullet-}$ was produced through the activation of peroxymonosulfate (PMS) by Co(II) ions at pH 8 in borate buffer. The reactivity of CDOM was studied based on the decrease in its ultraviolet absorbance at 254 nm (UVA_{254}) as a function of time. The reactivity of CDOM changed with time where fast and slow reacting CDOMs (i.e., $CDOM_{fast}$ and $CDOM_{slow}$) were clearly distinguished. A second-order rate constant of $CDOM_{fast}$ with $SO_4^{\bullet-}$ was calculated by plotting UVA_{254} decrease versus PMS exposure; where a R_{ct} value (i.e., ratio of sulfate radical to PMS exposure) was calculated using pCBA as a probe compound. The transformation of CDOM was studied through the analysis of the changes in UVA_{254}, electron donating capacity, fluorescence intensity, and total organic carbon. A transformation pathway leading to a significant carbon removal was proposed. This new knowledge on the kinetics and transformation of CDOM would ultimately assist in the development and operation of $SO_4^{\bullet-}$-based water treatment processes.

Keywords: Sulfate radical, CDOM, reaction kinetics, structural transformation, carbon removal

1. Introduction

Sulfate radical ($SO_4^{\bullet-}$)-based advanced oxidation processes (AOPs) have gained increasing interest in water treatment at both fundamental and applied levels (Siegrist et al. 2011, Wacławek et al. 2017). Due to its comparable or even stronger oxidizing capabilities than $^{\bullet}OH$, $SO_4^{\bullet-}$ is also capable of degrading a broad spectrum of trace organic contaminants (TOrCs) (e.g., pharmaceuticals, personal care products, and industrial chemicals) which are constantly detected in water bodies (Ghauch et al. 2017, Lutze et al. 2015a). A strong oxidation capacity, together with a high selectivity (i.e., lower scavenging of background organics) (Lutze et al. 2015a), multiple means of radical generation (Wang et al. 2014), and a favored storage/transport of stable solid precursors, make $SO_4^{\bullet-}$ a promising alternative for contaminants removal.

Previous studies focusing on the removal of TOrCs by $SO_4^{\bullet-}$ have provided key mechanistic and kinetic insights (Yang et al. 2019, Nihemaiti et al. 2018, Yang et al. 2017). However, little is known about the $SO_4^{\bullet-}$-induced reactivity and transformation of dissolved organic matter (i.e., DOM, a highly heterogeneous mixture of organic molecules ubiquitous in aquatic environments, and playing multiple key roles in water treatment) (Lutze et al. 2015a, Varanasi et al. 2018, Leenheer and Croué 2003). Briefly, the presence of DOM is known to decrease the removal efficiency of TOrCs due to its radical scavenging effect. Also, DOM transformation or removal can control disinfection byproducts formation or membrane fouling by applying $SO_4^{\bullet-}$-based AOPs as a pretreatment strategy (Chu et al. 2015, Xie et al. 2015, Cheng et al. 2017, Tian et al. 2018). Therefore, an advanced knowledge on

$SO_4^{\bullet-}$-induced reactivity and transformation of DOM is crucial to different water treatment processes considering its ubiquitous presence and the promising application of $SO_4^{\bullet-}$-based techniques.

The reactivity of DOM with oxidants such as chlorine, ozone, and $^{\bullet}OH$ has been extensively investigated. The difference in reactivity (i.e., faster reaction rate at the initial oxidation phase as compared to subsequent reaction phases) of different DOM isolates has been previously correlated with their structural variability and complexity (Chon et al. 2015, Westerhoff et al. 2004). Interestingly, while $^{\bullet}OH$ non-selectively reacts with target substances, $SO_4^{\bullet-}$ mainly reacts with electron rich aromatic or conjugated double bond moieties (Varanasi et al. 2018). This reactive DOM fraction has been termed as chromophoric dissolved organic matter (CDOM) due to its light absorbing property (Leenheer and Croué 2003, Lee et al. 2006). Therefore, the degradation rate of CDOM, as measured by ultraviolet absorbance at 254 nm (UVA_{254}) (Westerhoff et al. 2007), could be used to determine its reactivity to $SO_4^{\bullet-}$.

A detailed study on the transformation of DOM, as a result of its reactivity to $SO_4^{\bullet-}$, remains challenging due to its structural complexity and a lack of analytical techniques. Alternatively, traditional DOM characterization techniques could be applied to provide some insights into $SO_4^{\bullet-}$-induced changes of typical DOM characteristics, e.g., electron donating capacity (EDC), optical property (chromophoric or fluorescent property), molecular weight, or organic content (Li et al. 2016, Wang et al. 2017). For instance, an investigation on the transformation of DOM with $^{\bullet}OH$ was conducted by tracking the changes in chromophoric and fluorescent properties (Sarathy and Mohseni 2008). Specifically, the partial oxidation

(i.e., no significant carbon removal) of DOM led to the breakdown of larger molecules, ring open of aromatic structures and the formation of small organics. Interestingly, due to the favorable decarboxylation mechanism driven by $SO_4^{\bullet-}$, a higher DOM mineralization would be expected (Varanasi et al. 2018, Madhavan et al. 1978).

To fill this knowledge gap, the objective of this study was to investigate the reactivity and transformation of CDOM with $SO_4^{\bullet-}$. The reactivity of CDOM was studied by following the decrease of its UVA_{254} with time. A second order rate constant of fast reacting CDOM was calculated based on an established correlation between UVA_{254} and radical exposure. By recording the changes in UVA_{254}, electron donating capacity (EDC), fluorescence intensity (FI), and total organic carbon (TOC), information on CDOM transformation was obtained. A Co(II)-activated peroxymonosulfate (PMS) process was used for the production of $SO_4^{\bullet-}$ due to its high efficiency and simplicity. Four well characterized hydrophobic DOM fractions of different origins and characteristics were selected as model CDOM. This selection of organic isolates obtained from various sources shaping different characters represents a significant advance compared to model organics used in previous investigations.

2. Materials and method

2.1 Chemical reagents and DOM fractions

Peroxomonosufate (Oxone, $KHSO_5 \cdot 0.5KHSO_4 \cdot 0.5K_2SO_4$), 2,2'-azinobis (3-ethylbenzothiazoline-6-sulfonic acid) diammonium salt (ABTS; ≥98%), cobalt(II) sulfate (≥99.0%), sodium tetraborate (≥99.5%), ethanol (≥99.5%), and *tert*-butanol (pure) were purchased from Sigma-Aldrich and prepared with Ultrapure water (PURELAB Ultra, ELGA). Sulfuric acid of HPLC grade and sodium thiosulfate ($Na_2S_2O_3$) were purchased from UNIVAR. *p*-chlorobenzoic acid (pCBA, Acros Organics) was dissolved in ultrapure water to a concentration of 0.2 mM and used as a stock solution. A PMS stock solution of a high concentration (10 mM) was prepared and kept at 4°C due to its instability. The concentration of the stock solution was monitored on a daily basis prior to use.

Four DOM fractions previously isolated and characterized were selected for this study: Hydrophobic acids (i.e., DOM adsorbed onto XAD-8® resin at acid pH and eluted with sodium hydroxide) extracted from Suwannee River water (S-HPOA, USA) and Beaufort Reservoir (B-HPOA, France); hydrophobic DOM (i.e., similar protocol using a mixture of water and acetonitrile for resin elution) isolated from Ribou Reservoir NOM (R-HPO, France) and Colorado River (C-HPO, USA). The characteristics of the DOM isolates were summarized in table S1.

2.2 Experimental setup and procedures

Experiments were conducted in 40-mL amber glass vials with Teflon caps. A pre-determined amount of Co(II) as well as DOM stock solution were added into the 10 mM borate buffer to

obtain a final composition of 3.90 ± 0.11 mg C/L of DOM and 1 μM of Co(II) at pH 8. Instead of phosphate buffer, tetraborate was used as a buffer solution due to the reported complexing ability of the former with cobalt. A pH 8 buffer was used due to its improved buffering capacity upon the addition of PMS at high concentrations.

The experiments for CDOM reaction kinetics were started by introducing 1 mM PMS. The use of a high initial PMS concentration would allow for a study under both low and high PMS exposure conditions, representative of different water treatment processes. Ethanol and *tert*-butanol at different concentrations (1 or 10 mM) were used as radical quenching agents, while *p*CBA (10 μM) was used as a model compound to quantify primary reactive species. Samples were collected at specified time intervals and subjected to immediate measurement of PMS residual and UV absorbance at 254 nm (UVA_{254}) without the addition of quenching agent. The value of UVA_{254} was further corrected by subtracting the interferences from borate buffer (i.e., including H_2SO_4 for pH adjustment), $CoSO_4$, and PMS. Also, the contribution of PMS at each sampling time was calculated based on the residual PMS concentration and its ε_{254nm} measured in this study (12.3 $M^{-1}cm^{-1}$). For samples subjected to *p*CBA analysis, the reaction was stopped by adding 0.1 mL of ethanol (10 M) to 0.9 mL of sample. Sodium thiosulfate was found inefficient in quenching residual PMS with concentrations as high as 600 mM.

In order to avoid the interference of quenchers on Electron Donating Capacity (EDC) measurements, a new set of experiments was performed by using various initial PMS concentrations (i.e., from 0.00 to 1.00 mM) to achieve experimental conditions with different

PMS exposures. PMS residual was periodically monitored, and all samples were analyzed after complete PMS consumption. All experiments were performed at room temperature (20°C) in glass bottles installed on a rotary shaker (Ika-Werke GMBH & Co. (KG), Labortechnik KS250 Basic) operated at 500 rpm.

2.3. Analytical methods

2.3.1 Analysis of residual PMS

The concentration of PMS was measured by an $ABTS^{\bullet+}$-based method described elsewhere (Zhang et al. 2016). In this method, $ABTS^{\bullet+}$ is generated during the oxidation of ABTS by sulfate radical produced through the catalytic transformation of PMS, and then it was spectrophotometrically measured. Briefly, a solution containing 0.5 mL of ABTS (20 mM), 0.2 mL of $CoSO_4$ (20 mM), 10 mL of H_2SO_4 (2%), and 1 mL of water sample was well mixed and measured at a 734 nm wavelength with a spectrophotometer (Cary 60, Agilent). The calibration curve for PMS determination was shown in Fig. S1. A high concentration of $CoSO_4$ (20 mM) was applied to accelerate the catalytic decomposition of PMS. However, this interference has been taken into consideration with the measurement of a blank sample with no PMS addition, as suggested by the calibration curve in Figure S1. Also, a background DOM would not be influential due to a measurement recorded at 734nm.

2.3.2 Characterization of DOM transformation

The EDC of DOM samples was analysed based on a method developed by Chon et al (Chon et al. 2015). Briefly, a size exclusion chromatography (SEC) coupled with post column reaction was used, where $ABTS^{\bullet+}$ was produced by the oxidation of ABTS with sodium

persulfate in acidic environment. A TOYOPEARL HW-50S column (8mm×30cm) was selected for SEC using a 50 mM borate eluent (pH 7.8) at a flow rate of 0.2 mL/min. The post-column injection of $ABTS^{\bullet+}$ solution was operated at 0.05 mL/min from the helium pressurised generator. The reaction coil was connected to two UV detectors positioned in series (Agilent 1100 series, USA): the first one recording UV absorbance of DOM at 254 nm, and the second one recording the signal for $ABTS/ABTS^{\bullet+}$ at 405 nm.

A Cary 60 spectrophotometer (Agilent, USA) was used to collect absorbance data or to record the UV-vis spectra from 200 nm to 800 nm in 1cm path length quartz cell. The TOC concentration of each sample was measured with a Shimadzu TOC-L analyser (SHIDMAZU, Japan).

Fluorescence excitation and emission matrices (EEMs) were obtained using a Fluorescence spectrometer (Cary Eclipse, Varian). The operating parameters were adjusted based on the method from Chen et al (Chen et al. 2003). Briefly, the scan rate and excitation or emission slit bandwidth were set at 600 nm/min and 5nm, respectively. The spectra were recorded by scanning an emission spectra from 290 nm to 550 nm at a 5nm increment with the excitation wavelength ranging from 220 nm to 400 nm at a 5 nm increment.

The concentration of *p*CBA was measured with a HPLC unit equipped with a UV detector (Agilent 1100 series, USA) recording absorbance at 238 nm and with a 250 mm*4.6mm C18 5-µm reverse phase column (Alltima™, GRACE). The mobile phase consisted of 60% methanol and 40% phosphoric acid (0.1%, V/V). The *p*CBA calibration curve was built using gradually diluted stock solution.

185

3. Results and Discussion

3.1 Biphasic decrease of CDOM in Co(II)/PMS system

The reaction of CDOM with PMS led to an average decrease of 11% in UVA_{254} within 60 min (Fig. S2). However, the decrease of UVA_{254} was remarkably faster in the presence of both PMS and Co(II) (Fig. 1). Approximately 55% to 70% decrease in UVA_{254} (depending on the DOM fraction) was observed in Co(II)-catalyzed PMS system within 60 min. This enhanced reaction was caused by the generation of reactive species (e.g., $SO_4^{\bullet-}$) in the Co(II)/PMS system, while the slight UVA_{254} decrease in the absence of Co(II) catalyst was probably due to the reaction of quinones with PMS as previously reported (Zhou et al. 2015). The occurrence of quinones within humic substances has been widely acknowledged (Cory and McKnight 2005).

Fig. 1.

Noticeably, a fast and slow reaction phase could be distinguished for all DOM fractions throughout the oxidation process (Fig. 1). Specifically, the pseudo-first-order rate constants of the fast reaction phase were 4.2 to 6.9 times higher than the rate constants of the slower reaction phase. These results showed a significant difference in the reactivity of CDOM with $SO_4^{\bullet-}$ due to the heterogeneous structural property of the organic matter isolates. It has been previously reported that aromatic structures substituted with electron donating groups (i.e., –OH, $–NH_3$, $–OCH_3$) exhibited higher reactivity to $SO_4^{\bullet-}$ (Luo et al. 2017); these structures could represent the main contributor to the fast reacting CDOM (i.e., $CDOM_{fast}$). The slow

reacting CDOM (i.e., $CDOM_{slow}$) might include lower electron density moieties from the original CDOM constituents as well as the oxidation products of $CDOM_{fast}$ (Xiao et al. 2015, Zhang et al. 2012).

The influence of the aromatic character of the DOM fractions on their reactivity with $SO_4^{\bullet-}$ was highly expected based on previous findings (Westerhoff et al. 2004, Luo et al. 2017). However, the difference in reactivity among the four DOM fractions was more significant during the slow reaction phase. The pseudo-first-order reaction rates of $CDOM_{slow}$ (i.e., $\ln(UVA_{254}/UVA_{254,0})$ versus reaction time) were calculated as 1.20×10^{-2}, 0.84×10^{-2}, 0.63×10^{-2}, and 0.46×10^{-2} min^{-1} for S-HPOA, B-HPOA, R-HPO and C-HPO, respectively. These $CDOM_{slow}$ reactivities linearly increased with the SUVA values as shown in Fig. S3. The $CDOM_{fast}$ reactivity to $SO_4^{\bullet-}$ of the four DOM fractions was further discussed in the following sections.

3.2 Evaluation of sulfate radical production

Anipsitakis and Dionysiou (Anipsitakis and Dionysiou 2003) reported the predominant role of $SO_4^{\bullet-}$ (eq. 1) over $^{\bullet}OH$ in Co(II)-catalyzed PMS systems at pH 7. Because a pH 8 may promote a higher production of $^{\bullet}OH$ (eq. 2), the identification of major oxidizing species in the current system was conducted by following the degradation of *p*CBA as a probe compound under different scavenging conditions (Lutze et al. 2015b). The second-order rate constants of *p*CBA and radical scavengers (i.e., *t*-BuOH and EtOH) with $^{\bullet}OH$ and $SO_4^{\bullet-}$ were summarized in table S3. When 10 mM of radical scavenger (i.e., *t*-BuOH or EtOH, at a molar ratio of 1000:1 versus *p*CBA) was applied, the *p*CBA removal efficiency was decreased by

approximately 10% in the presence of *t*-BuOH; while almost no *p*CBA decrease was observed with the addition of EtOH (Fig. S4). Quantitatively, the ratio of the measured concentration of $^{\bullet}OH$ to $SO_4^{\bullet-}$was lower than 3%. These results indicated that $SO_4^{\bullet-}$ was the predominant reactive species at pH 8. This is probably due to the competition for $SO_4^{\bullet-}$ by either pCBA (3.6×10^8 $M^{-1}s^{-1}$) or scavengers (i.e., DOM fractions, up to 10^8 $M^{-1}s^{-1}$ as discussed below), leading to the unfavorable production of $^{\bullet}OH$ (eq 2).

$$HSO_5^- + Co^{2+} = SO_4^{\bullet-} + Co^{3+} + OH^- \quad (1)$$

$$SO_4^{\bullet-} + OH^- = SO_4^- + {}^{\bullet}OH \left(k_{SO_4^{\bullet-},\,OH^-} = 6.5\times10^7 M^{-1}s^{-1}\right) \quad (2)$$

$$HSO_5^- + Co^{3+} = SO_5^{\bullet-} + Co^{2+} + H^+ \quad (3)$$

Therefore, the production of $SO_4^{\bullet-}$ was investigated following the R_{ct} concept and the analysis of *p*CBA decay. R_{ct} (i.e., the ratio of radical exposure to oxidant exposure) (Elovitz and von Gunten 1999) was used to present the production of $SO_4^{\bullet-}$ with PMS exposure (eq. 4). According to Elovitz and von Gunten (Elovitz and von Gunten 1999), the consumption of radicals by a probe compound (P) (e.g., *p*CBA in the current study) is considered insignificant as compared to major radical scavengers (S) (e.g., DOM in current study) if the probe compound is present at a considerably low concentration (i.e., $k_P[P] << k_S[S]$, where k_P and k_S represents the rate constants of the probe compound and major radical scavengers with radicals, respectively). Therefore, a low *p*CBA concentration (i.e., 1 μM) was applied to

ensure an insignificant radical consumption by *p*CBA as compared to DOM. Specifically, k_{pCBA}[*p*CBA] was calculated as approximately 1.4% of k_{DOM}[DOM] under the current experimental condition, where k_{pCBA} and k_{DOM} represent the second order rate constants of *p*CBA (3.6×10^8 $M^{-1}s^{-1}$) and DOM (6.8×10^3 $LmgC^{-1}s^{-1}$) with $SO_4^{\bullet-}$, respectively. The R_{ct} value was only studied for the first 10 min of the reaction. $CDOM_{fast}$ was observed reactive within this timeframe (Fig. 1). The conversion from reaction time to PMS exposure was illustrated in Table S4.

Although no noticeable interference was observed with UVA_{254} or EDC measurements, the rate of catalytic PMS decomposition decreased (Fig. S5) due to the formation of cobalt-DOM complex. For instance, a 57% PMS decomposition was observed within 60 min in the DOM-free system. However, the PMS decomposition values for S-HPOA-, B-HPOA-, R-HPO-, and C-HPO-containing system were 41%, 43%, 40%, and 43%, respectively. Specifically, approximately 80% of Co(II) was calculated as forming complexes with DOM under the current experimental conditions using the NICA-Donnan model with the constants adapted from Milne et al (Milne et al. 2003). In DOM-containing solutions with the addition of *p*CBA as probe compound, PMS decomposed following a pseudo-first-order reaction (Fig. S6a), as described by (eq. 5), and k (i.e., pseudo-first-order rate constant) was measured as approximately $3.0\times10^{-4}s^{-1}$ independent of DOM origins. The influence of *p*CBA addition (1 μM) on PMS decomposition was negligible. For instance, the averaged PMS residual measured in different DOM-containing systems within 10 min was 80% in the absence of *p*CBA (Figure S5) and 79% in the presence of *p*CBA (Figure S6a). The determined rate

(within 10 min) was predominantly contributed by a catalytic decomposition since self-decomposition of PMS was found negligible within 2 hr at room temperature (20°C). The degradation of *p*CBA (Fig. S6b) caused by $SO_4^{\bullet-}$ was described by eq. 6 and 7. By combining eq. 4 and 5, *p*CBA degradation could be described using the R_{ct} concept (eq. 8).

$$R_{ct} = \frac{\int_0^t [SO_4^{\bullet-}]\mathrm{dt}}{\int_0^t [PMS]\mathrm{dt}} \quad (4)$$

$$[PMS] = [PMS]_0 e^{-kt} \quad (5)$$

$$-\frac{\mathrm{d}[pCBA]}{dt} = k_{SO_4^{\bullet-},\,pCBA}[pCBA][SO_4^{\bullet-}] \quad (6)$$

$$\ln\frac{[pCBA]}{[pCBA]_0} = -k_{SO_4^{\bullet-},\,pCBA}\int_0^t [SO_4^{\bullet-}]\mathrm{dt} \quad (7)$$

$$\ln\frac{[pCBA]}{[pCBA]_0} = -k_{SO_4^{\bullet-},\,pCBA}R_{ct}[PMS]_0\int_0^t \mathrm{e}^{-\mathrm{kt}}\mathrm{dt} \quad (8)$$

By plotting ln (*p*CBA/*p*CBA$_0$) versus PMS exposure, linear correlations were observed as a function of PMS exposures (Fig. 2). The R_{ct} value at PMS exposures higher than 0.1 M·s (i.e. a reaction time of 2–10 min, table S4) for each system was determined from the slope of the linear regression line (Fig. 2) and listed in Table 1; while the higher R_{ct} values at PMS exposures lower than 0.1 M·s (i.e. a reaction time of 0–2 min, table S4) were shown in Fig.

S7. Higher R_{ct} values at the initial oxidation stage (PMS exposure < 0.1 M·s, results discussed in section 3.4.1) have also been reported during the ozonation of surface waters (Elovitz and von Gunten 1999). The change of R_{ct} in the current study was likely due to the Co(II) regeneration process. Specifically, the conversion of Co(II) to Co(III) with a precipitate formation of the latter has been considered as a probable explanation for the slowing down of the catalytic rate with time at pH above 5.9 (Zhang and Edwards 1992). With a pH of 8 used in this study, Co(III) might have also precipitated out as $Co(OH)_3$ (K_{sp} = 1.6×10^{-44}), leading to the retardation of the regeneration process and consequently to a slower $SO_4^{\bullet-}$ production. Moreover, the additional PMS consumption during the regeneration of Co(II) (eq. 3), which inefficiently produced $SO_5^{\bullet-}$ (Neta et al. 1988), would also lead to a decreased R_{ct}. A change in Co(II) catalytic behavior at different pH probably associated with Co(III) precipitation at higher pH has also been observed in previous studies. For instance, the degradation rate of 2,4-DCP in Co(II)/PMS system slowed down with reaction time at pH 7 (Anipsitakis et al. 2005), while it remained unaffected at pH 2 (Anipsitakis and Dionysiou 2003). Considering that no enhanced UVA_{254} decrease (explained in Section 3.4.1) was observed (Fig. 1) in contrast to the significantly higher *p*CBA degradation (Fig. S6b) at the initial oxidation stage (i.e., PMS exposure lower than 0.1 M·s), the relatively lower R_{ct} values (Table 1) determined after the initial short stage were used in the analysis of the following section.

Fig. 2.

Table 1.

3.3 Reactivity of $CDOM_{fast}$ to $SO_4^{\bullet-}$ and its application

Fig. 3.

Following the procedures for establishing a relationship between ln ($pCBA/pCBA_0$) and PMS exposure (eq. 8), i.e., obtained by combining eq.(4), eq.(5) and eq.(7)), a similar correlation was also established between $\ln(UVA_{254}/UVA_{254,0})$ of $CDOM_{fast}$ and PMS exposure (eq. 9). This correlation was found linear when $\ln(UVA_{254}/UVA_{254,0})$ of $CDOM_{fast}$ was plotted against PMS exposure for all DOM fractions (Fig. 3). The good linearity allowed the calculation of the reaction rate constant of $CDOM_{fast}$ with $SO_4^{\bullet-}$ using the R_{ct} value determined in Section 3.2.

$$\ln\frac{[UVA_{254}]}{[UVA_{254}]_0} = -k_{SO_4^{\bullet-},\,CDOM} R_{ct} [PMS]_0 \int_0^t e^{-kt} dt \quad (9)$$

Interestingly, the reaction rate constants of $CDOM_{fast}$ for all DOM fractions were at the same order of magnitude. The highest $CDOM_{fast}$ value was recorded for S-HPOA (4.59×10^8 $M^{-1}s^{-1}$), also exhibiting the highest SUVA (4.78). The lowest $CDOM_{fast}$ value was observed for C-HPO (1.99×10^8 $M^{-1}s^{-1}$), also showing lowest SUVA (2.14). However, B-HPOA (SUVA: 4.06) showed a lower k value than R-HPO (SUVA: 3.22), i.e., 3.04×10^8 $M^{-1}s^{-1}$ versus 3.48×10^8 $M^{-1}s^{-1}$, respectively. Therefore, the correlation between the reactivity of $CDOM_{fast}$ and SUVA of the corresponding DOM fraction would need additional investigation by including a larger pool of DOM fractions. These reaction rate constants were one order of magnitude higher than the data previously reported (i.e., ~$10^7 M_C^{-1}s^{-1}$). For instance, Lutz et al (Lutze et al. 2015a) observed a rate of 6.8×10^3 $L mgC^{-1}s^{-1}$ for humic acid (Depur from

Carl Roth) using an indirect kinetic competition method; while Zhou et al (Zhou et al. 2017) recorded a rate of 1.86×10^3 $LmgC^{-1}s^{-1}$ for Suwannee River fulvic acid using a direct laser flash photolysis method. The difference could be attributed to the fact that the value in this study was only measured for the conceptually isolated fast reacting moieties (i.e., $CDOM_{fast}$) rather than for the bulk DOM (i.e., a combination of both fast and slow reacting moieties). However, the value was one order of magnitude lower than those reported for aromatic compounds (~10^9 $M^{-1}s^{-1}$) (Neta et al. 1977, Fischer and Radom 2001). This difference would be the result of stronger electrosteric repulsion between $SO_4^{\bullet-}$ and structurally complex DOM as compared to simpler organic compounds. The higher reactivity of sulfate radicals to $CDOM_{fast}$ than to OH^- (~$10^7 M^{-1}s^{-1}$) was expected to lead to an insignificant production of $^{\bullet}OH$ (eq. 2) due to its unfavorable formation kinetics. In addition, $CDOM_{fast}$ would be preferred to bulk DOM when evaluating the scavenging property of dissolved organic matter in $SO_4^{\bullet-}$-based AOPs under lower PMS exposures, where $CDOM_{fast}$ was the major reactive moieties (Fig. 1).

The use of UVA_{254} as a surrogate indicator for the assessment of TOrCs removal efficiency has been extensively studied in ozone- and $^{\bullet}OH$-based AOPs (Gerrity et al. 2012, Rosario-Ortiz et al. 2010, Li et al. 2017). This finding could also support its application in $SO_4^{\bullet-}$-based water treatment processes. The study on TOrCs removal efficiency could be achieved using either: i) the kinetics with second order reaction constants of TOrCs and radical exposure (eq. 10), or ii) the correlation established between UVA_{254} decrease and contaminants removal (eq. 11).

$$\ln\frac{[TOrCs]}{[TOrCs]_0} = -k_{SO_4^{\bullet-},\,TrOCs}\int_0^t SO_4^{\bullet-}\mathrm{dt} = -k_{SO_4^{\bullet-},\,TrOCs}\ln\frac{[UVA_{254}]}{[UVA_{254}]_0} / -k_{SO_4^{\bullet-},\,CDOM} \quad (10)$$

$$\ln\frac{[TOrCs]}{[TOrCs]_0} = Slope\times\ln\frac{[UVA_{254}]}{[UVA_{254}]_0} + Intercept \quad (11)$$

As compared to the direct measurement of TOrCs in a full-scale water treatment plant, the indirect monitoring of UV absorbing parameters using spectrophotometer would require lower capital/operating cost as well as time input. Especially, with the use of an on-line spectrophotometer, a quick track of the oxidation efficiency and consequently a rapid adjustment (i.e., oxidant dose or contact time) could also be expected. However, different correlation models should be established for different TOrCs due to the discrepancy in their reactivity. The successful application of this correlation could also be impacted by the fluctuation of water matrices (e.g., HCO_3^-, NO_3^-, or Cl^-) or temperature due to seasonal changes.

The use of UV absorbing indices of humic substances in combination with their fluorescence properties has also been suggested as indicators in ozone-based water treatment processes (Li et al. 2017). However, similar decreasing trend was observed in the current study between UVA_{254} and fluorescence intensity with increasing PMS concentration (Text S1). Consequently, the UVA_{254} parameter was sufficient as a single process indicator in this $SO_4^{\bullet-}$-based oxidation system.

3.4 Sulfate radical-induced CDOM transformation

3.4.1 EDC decrease as a function of PMS exposures

Fig. 4.

372 Electron donating capacity (EDC) associated with the presence of phenolic structures with
373 different degree of substitution has been previously reported for aquatic humic substances
374 (Aeschbacher et al. 2012). The change in EDC (Fig. S8) was studied for each DOM fraction
375 under various PMS exposures. The different PMS exposures were obtained by applying
376 varying initial PMS concentrations for the same contact time (i.e., 20 h) and the calculation of
377 the PMS exposures was detailed in Text S2, SI. In addition, the changes in normalized EDC
378 and UVA_{254} (Fig. S9) of the four DOM fractions were plotted in Fig. 4. This figure shows that
379 for PMS exposures lower than 0.1 M·s (Area a_1), an average of 54% decrease of EDC was
380 recorded when only a 30% decrease of UVA_{254} was observed. For PMS exposures higher
381 than 0.1 M·s (Area b), the averaged normalized UVA_{254} decreased from 70% to 13% (i.e., a
382 57% decrease), whereas the averaged normalized EDC decreased from 46% to 7% (i.e., a 39%
383 decrease). The larger decrease of EDC than UVA_{254} at PMS exposure lower than 0.1 M·s in
384 this system indicated that the initial phase of $SO_4^{\bullet-}$ reaction was the oxidation of phenolics
385 into quinone-type structures with similar chromophoric properties (Ramseier and Gunten
386 2009). This reaction is thermodynamically favourable considering the very low oxidation
387 potential of phenolic structures (0.153–0.620 V) (Bortolomeazzi et al. 2007) and the strong
388 reduction potential of sulfate radicals (2.5–3.1V) (Anipsitakis and Dionysiou 2003). A similar
389 observation has been previously reported during the treatment of humic substances by ClO_2
390 or HClO, where hydroquinone or catechol moieties (i.e., major EDC contributors (Chon et al.
391 2015)) were proposed as oxidized by HClO through electron transfer rather than electrophilic
392 substitution (Wenk et al. 2013). Interestingly, a more pronounced decrease in EDC than in

393 UVA_{254} was observed with a PMS exposure lower than 0.01 M·s (Area a_0, Fig. 4), which was
394 probably caused by the relatively higher R_{ct} observed under this condition (Fig. S7).
395 Due to a major $SO_4^{\bullet-}$consumption by the moieties with EDC at the initial oxidation phase
396 (i.e., PMS exposure < 0.1 M·s), a UVA_{254} decrease was not enhanced even under higher
397 radical exposure (i.e., higher R_{ct}) (Fig. 3). This result supported the selection of lower R_{ct}
398 values (Fig. 2) in the calculation of the second-order rate constants of $CDOM_{fast}$ with $SO_4^{\bullet-}$ as
399 described in section 3.3.

400 ***3.4.2 TOC removal efficiency at various PMS exposures***

401 **Fig. 5.**

402 In order to further explore the transformation of CDOM by sulfate radicals, the TOC content
403 of the solution under different PMS exposures was measured. A significant TOC removal,
404 64%, 63%, 56%, 49% for S-HPOA, B-HPOA, R-HPO and C-HPO, respectively (i.e., 58% in
405 average), was observed under a PMS exposure of 8.04 M·s (Fig. S10). The relationship
406 between UVA_{254} decrease and TOC removal was established and shown in Fig. 5.
407 Interestingly, the TOC removal was minor (i.e., less 10%) during the depletion of the UV
408 absorbance of $CDOM_{fast}$ (i.e., UVA_{254} decrease within 50%, as indicated by the red dashed
409 line in Fig. 5). However, the decrease in the chromophoric property of $CDOM_{slow}$ (i.e.,
410 observed when UVA_{254} decrease was larger than 50%, right side of the red dashed line in Fig.
411 5) led to a considerable TOC removal. These results indicated that the reaction of $CDOM_{fast}$
412 would mainly lead to the breakdown of complex aromatic structures into small molecular
413 weight fractions with insignificant mineralization. This transformation from larger molecules

414 to smaller ones was evidenced by the blue shift or band contraction (Chen et al. 2002) in
415 fluorescence emission spectra (Fig. 6). Specifically, the decrease in the band width at 1/2
416 maximum fluorescence intensity was calculated as 24 nm, 24 nm, 33 nm, and 88 nm for
417 S-HPOA, B-HPOA, R-HPO, and C-HPO, respectively. In contrast, the reaction of $CDOM_{slow}$
418 would mainly undergo through decarboxylation, which directly led to the observed carbon
419 removal.

420 **Fig. 6.**

421 Interestingly, a good linearity between UVA_{254} decrease and TOC removal during the
422 $CDOM_{slow}$ decrease was observed (Fig. 5). These results indicated that the change in
423 $CDOM_{slow}$ could be used in the prediction of TOC removal for surface water during
424 $SO_4^{\bullet-}$-based treatment. This may include water treatment processes targeting the removal of
425 organics, e.g., pretreatment for the removal of disinfection byproducts precursors or
426 membranes foulants, membrane cleaning, and the treatment of reverse osmosis concentrates.
427 Nevertheless, under different water matrices this correlation might be affected by pH
428 conditions, or the presence of radical scavengers HCO_3^- or Cl^-.

429 ***3.4.3 Evolution of CDOM transformation with sulfate radical***

430 Based on the findings of this study (i.e., results obtained with the current characterization
431 techniques), the evolution of the transformation of CDOM by sulfate radicals was
432 summarized in Fig. 7. The $SO_4^{\bullet-}$-induced reaction of $CDOM_{fast}$, (i.e., electron donating group
433 substituted aromatic structures) was mainly initiated through single electron transfer or

addition. The depletion of EDC would initially take place through the electron transfer from phenolic hydroxyl groups to sulfate radical as suggested by Reaction 1. Reaction 2 would produce hydroxylated C-centered radical cations and consequently lead to the formation of ring cleavage products (Anipsitakis et al. 2006). Remarkably, Reaction 4 would take place due to the high electron density at R_3 site leading to the formation of smaller fluorescent molecules, as suggested by the blue shift of fluorescence emission spectra (Fig. 6). The production of smaller molecules from complex structures could also be evidenced by the increased fluorescence signal (Figure S13) at lower PMS exposure, as the smaller aromatic moieties would be more fluorescent due to weaker intramolecular quenching effect. The decarboxylation of carboxyl groups (Reaction 3), i.e., newly formed or originally incorporated within DOM structures, would be the main reaction mechanism of $CDOM_{slow}$ transformation (Madhavan et al. 1978) leading to a significant removal of TOC. However, a more detailed study would be highly recommended for the optimization of process conditions for maximum carbon removal.

Fig. 7.

4. Conclusions

The current study provided systematic information on both the reactivity and fate of CDOM with sulfate radical. DOM fractions with different origins and characteristics were used in this investigation. The main conclusions included:

- Fast and slow reacting CDOM could be distinguished within all DOM fractions. Interestingly, the difference in the reactivity of $CDOM_{fast}$ among different organics were minor, while the reactivity $CDOM_{slow}$ were observed to increase with SUVA.

- The reactivity of $CDOM_{fast}$ to $SO_4^{\bullet-}$ was calculated at an order of $10^8\ M^{-1}s^{-1}$ from the observed linear correlation between $CDOM_{fast}$ decrease and sulfate radical exposure. The correlation also validated the potential application of UVA_{254} as a surrogate indicator for TOrCs removal efficiency.

- A faster decrease of EDC than UVA_{254} at lower PMS exposure indicated a preferred oxidation of phenolic structures (i.e., preferential decrease of Electron Donating Capacity). Afterwards, the oxidation of $CDOM_{fast}$ would proceed with the formation of transient intermediates and ring cleavage products.

- The transformation products of $CDOM_{fast}$ together with the originally less reactive structures, i.e., $CDOM_{slow}$, would undergo slow decarboxylation leading to a significant carbon removal. The linear relationship recorded between $CDOM_{slow}$ reduction and TOC removal could be used to predict carbon removal.

The findings in this work would highly assist in the design and operation of $SO_4^{\bullet-}$- based water treatment processes. Specifically, the scavenging capacity of background DOM could be better evaluated using the calculated reactivity of $CDOM_{fast}$ if the applied PMS exposure would mainly cause changes in $CDOM_{fast}$. Also, the correlation established between CDOM and radical exposure would shed light on the applicability of UVA_{254} as an indicator of TOrCs

473 removal efficiency in $SO_4^{\bullet-}$-based water treatment processes. However, further site-specific
474 studies on the use of UVA_{254} as an indicator are highly needed for its successful application.
475 $SO_4^{\bullet-}$-based advanced oxidation technique could be developed to address the need for DOM
476 removal in varying water treatment scenarios, e.g., pretreatment for the removal of disinfection
477 by-products precursors or membrane foulants, application of catalytic membrane for organic
478 fouling mitigation, membrane cleaning, or the treatment of reverse osmosis concentrate
479 produced from reclaimed water treatment plants. Also, an increased PMS dose could be
480 applied to increase the reaction rate of $CDOM_{slow}$ and consequently increase carbon removal.
481 In addition, carbon removal efficiency could be simply estimated based on the removal of
482 $CDOM_{slow}$ due to the observed good correlation.

483 Acknowledgements

484 China Scholarship Council (CSC) and Curtin University are acknowledged for providing the
485 CSC-Curtin joint PhD scholarship to Suona Zhang.

486 Appendix A. Supplementary information

487 Supplementary information related to this article could be found in a separate Microsoft Word
488 document (Supplementary Information).

References

Siegrist, R.L., Crimi, M. and Simpkin, T.J. (2011) In situ chemical oxidation for groundwater remediation, Springer Science & Business Media.

Wacławek, S., Lutze, H.V., Grübel, K., Padil, V.V.T., Černík, M. and Dionysiou, D.D. (2017) Chemistry of persulfates in water and wastewater treatment: A review. Chemical Engineering Journal 330, 44-62.

Ghauch, A., Baalbaki, A., Amasha, M., El Asmar, R. and Tantawi, O. (2017) Contribution of persulfate in UV-254 nm activated systems for complete degradation of chloramphenicol antibiotic in water. Chemical Engineering Journal 317, 1012-1025.

Lutze, H.V., Bircher, S., Rapp, I., Kerlin, N., Bakkour, R., Geisler, M., von Sonntag, C. and Schmidt, T.C. (2015a) Degradation of Chlorotriazine Pesticides by Sulfate Radicals and the Influence of Organic Matter. Environmental Science & Technology 49(3), 1673-1680.

Wang, Y., Le Roux, J., Zhang, T. and Croué, J.-P. (2014) Formation of Brominated Disinfection Byproducts from Natural Organic Matter Isolates and Model Compounds in a Sulfate Radical-Based Oxidation Process. Environmental Science & Technology 48(24), 14534-14542.

Yang, Y., Cao, Y., Jiang, J., Lu, X., Ma, J., Pang, S., Li, J., Liu, Y., Zhou, Y. and Guan, C. (2019) Comparative study on degradation of propranolol and formation of oxidation products by UV/H2O2 and UV/persulfate (PDS). Water Research 149, 543-552.

Nihemaiti, M., Miklos, D.B., Hübner, U., Linden, K.G., Drewes, J.E. and Croué, J.-P. (2018) Removal of trace organic chemicals in wastewater effluent by UV/H2O2 and UV/PDS. Water Research 145, 487-497.

Yang, Y., Lu, X., Jiang, J., Ma, J., Liu, G., Cao, Y., Liu, W., Li, J., Pang, S., Kong, X. and Luo, C. (2017) Degradation of sulfamethoxazole by UV, UV/H2O2 and UV/persulfate (PDS): Formation of oxidation products and effect of bicarbonate. Water Research 118, 196-207.

Varanasi, L., Coscarelli, E., Khaksari, M., Mazzoleni, L.R. and Minakata, D. (2018) Transformations of dissolved organic matter induced by UV photolysis, Hydroxyl radicals, chlorine radicals, and sulfate radicals in aqueous-phase UV-Based advanced oxidation processes. Water Research 135, 22-30.

Leenheer, J.A. and Croué, J.-P. (2003) Peer Reviewed: Characterizing Aquatic Dissolved Organic Matter. Environmental Science & Technology 37(1), 18A-26A.

Chu, W., Li, D., Gao, N., Templeton, M.R., Tan, C. and Gao, Y. (2015) The control of emerging haloacetamide DBP precursors with UV/persulfate treatment. Water Research 72, 340-348.

Xie, P., Ma, J., Liu, W., Zou, J. and Yue, S. (2015) Impact of UV/persulfate pretreatment on the formation of disinfection byproducts during subsequent chlorination of natural organic matter. Chemical Engineering Journal 269, 203-211.

Cheng, X., Liang, H., Ding, A., Tang, X., Liu, B., Zhu, X., Gan, Z., Wu, D. and Li, G. (2017) Ferrous iron/peroxymonosulfate oxidation as a pretreatment for ceramic ultrafiltration membrane: Control of natural organic matter fouling and degradation of atrazine. Water Research 113, 32-41.

Tian, J., Wu, C., Yu, H., Gao, S., Li, G., Cui, F. and Qu, F. (2018) Applying ultraviolet/persulfate (UV/PS) pre-oxidation for controlling ultrafiltration membrane fouling by natural organic matter (NOM) in surface water. Water Research 132, 190-199.

Chon, K., Salhi, E. and von Gunten, U. (2015) Combination of UV absorbance and electron donating capacity to assess degradation of micropollutants and formation of bromate during ozonation of wastewater effluents. Water Research 81, 388-397.

Westerhoff, P., Chao, P. and Mash, H. (2004) Reactivity of natural organic matter with aqueous chlorine and bromine. Water Research 38(6), 1502-1513.

Lee, N., Amy, G. and Croue, J.-P. (2006) Low-pressure membrane (MF/UF) fouling associated with allochthonous versus autochthonous natural organic matter. Water Research 40(12), 2357-2368.

Westerhoff, P., Mezyk, S.P., Cooper, W.J. and Minakata, D. (2007) Electron Pulse Radiolysis Determination of Hydroxyl Radical Rate Constants with Suwannee River Fulvic Acid and Other Dissolved Organic Matter Isolates. Environmental Science & Technology 41(13), 4640-4646.

Li, T., Jiang, Y., An, X., Liu, H., Hu, C. and Qu, J. (2016) Transformation of humic acid and halogenated byproduct formation in UV-chlorine processes. Water Research 102, 421-427.

Wang, W.-L., Zhang, X., Wu, Q.-Y., Du, Y. and Hu, H.-Y. (2017) Degradation of natural organic matter by UV/chlorine oxidation: Molecular decomposition, formation of oxidation byproducts and cytotoxicity. Water Research 124, 251-258.

Sarathy, S. and Mohseni, M. (2008) The fate of natural organic matter during UV/H2O2 advanced oxidation of drinking water. Canadian Journal of Civil Engineering 36(1), 160-169.

Madhavan, V., Levanon, H. and Neta, P. (1978) Decarboxylation by $SO_4^{\cdot-}$ Radicals. Radiation Research 76(1), 15-22.

Zhang, T., Chen, Y. and Leiknes, T. (2016) Oxidation of refractory benzothiazoles with PMS/CuFe2O4: kinetics and transformation intermediates. Environmental Science & Technology 50(11), 5864-5873.

Chen, W., Westerhoff, P., Leenheer, J.A. and Booksh, K. (2003) Fluorescence Excitation−Emission Matrix Regional Integration to Quantify Spectra for Dissolved Organic Matter. Environmental Science & Technology 37(24), 5701-5710.

Zhou, Y., Jiang, J., Gao, Y., Ma, J., Pang, S.-Y., Li, J., Lu, X.-T. and Yuan, L.-P. (2015) Activation of Peroxymonosulfate by Benzoquinone: A Novel Nonradical Oxidation Process. Environmental Science & Technology 49(21), 12941-12950.

Cory, R.M. and McKnight, D.M. (2005) Fluorescence Spectroscopy Reveals Ubiquitous Presence of Oxidized and Reduced Quinones in Dissolved Organic Matter. Environmental Science & Technology 39(21), 8142-8149.

Luo, S., Wei, Z., Dionysiou, D.D., Spinney, R., Hu, W.-P., Chai, L., Yang, Z., Ye, T. and Xiao, R. (2017) Mechanistic insight into reactivity of sulfate radical with aromatic contaminants through single-electron transfer pathway. Chemical Engineering Journal 327, 1056-1065.

571 Xiao, R., Ye, T., Wei, Z., Luo, S., Yang, Z. and Spinney, R. (2015) Quantitative Structure–
572 Activity Relationship (QSAR) for the Oxidation of Trace Organic Contaminants by
573 Sulfate Radical. Environmental Science & Technology 49(22), 13394-13402.
574 Zhang, H., Zhang, Y., Shi, Q., Ren, S., Yu, J., Ji, F., Luo, W. and Yang, M. (2012)
575 Characterization of low molecular weight dissolved natural organic matter along the
576 treatment trait of a waterworks using Fourier transform ion cyclotron resonance mass
577 spectrometry. Water Research 46(16), 5197-5204.
578 Anipsitakis, G.P. and Dionysiou, D.D. (2003) Degradation of Organic Contaminants in Water
579 with Sulfate Radicals Generated by the Conjunction of Peroxymonosulfate with Cobalt.
580 Environmental Science & Technology 37(20), 4790-4797.
581 Lutze, H.V., Kerlin, N. and Schmidt, T.C. (2015b) Sulfate radical-based water treatment in
582 presence of chloride: Formation of chlorate, inter-conversion of sulfate radicals into
583 hydroxyl radicals and influence of bicarbonate. Water Research 72, 349-360.
584 Elovitz, M.S. and von Gunten, U. (1999) Hydroxyl Radical/Ozone Ratios During Ozonation
585 Processes. I. The Rct Concept. Ozone: Science & Engineering 21(3), 239-260.
586 Milne, C.J., Kinniburgh, D.G., Van Riemsdijk, W.H. and Tipping, E. (2003) Generic NICA–
587 Donnan model parameters for metal-ion binding by humic substances. Environmental
588 Science & Technology 37(5), 958-971.
589 Zhang, Z. and Edwards, J.O. (1992) Chain lengths in the decomposition of
590 peroxomonosulfate catalyzed by cobalt and vanadium. Rate law for catalysis by
591 vanadium. Inorganic Chemistry 31(17), 3514-3517.
592 Neta, P., Huie, R.E. and Ross, A.B. (1988) Rate constants for reactions of inorganic radicals
593 in aqueous solution. Journal of Physical and Chemical Reference Data 17(3), 1027-1284.
594 Anipsitakis, G.P., Stathatos, E. and Dionysiou, D.D. (2005) Heterogeneous activation of
595 Oxone using Co 3O 4. Journal of Physical Chemistry B 109(27), 13052-13055.
596 Zhou, L., Sleiman, M., Ferronato, C., Chovelon, J.-M. and Richard, C. (2017) Reactivity of
597 sulfate radicals with natural organic matters. Environmental Chemistry Letters 15(4),
598 733-737.
599 Neta, P., Madhavan, V., Zemel, H. and Fessenden, R.W. (1977) Rate constants and
600 mechanism of reaction of sulfate radical anion with aromatic compounds. Journal of the
601 American Chemical Society 99(1), 163-164.
602 Fischer, H. and Radom, L. (2001) Factors Controlling the Addition of Carbon-Centered
603 Radicals to Alkenes—An Experimental and Theoretical Perspective. Angewandte Chemie
604 International Edition 40(8), 1340-1371.
605 Gerrity, D., Gamage, S., Jones, D., Korshin, G.V., Lee, Y., Pisarenko, A., Trenholm, R.A.,
606 von Gunten, U., Wert, E.C. and Snyder, S.A. (2012) Development of surrogate correlation
607 models to predict trace organic contaminant oxidation and microbial inactivation during
608 ozonation. Water Research 46(19), 6257-6272.
609 Rosario-Ortiz, F.L., Wert, E.C. and Snyder, S.A. (2010) Evaluation of UV/H2O2 treatment
610 for the oxidation of pharmaceuticals in wastewater. Water Research 44(5), 1440-1448.
611 Li, W.-T., Cao, M.-J., Young, T., Ruffino, B., Dodd, M., Li, A.-M. and Korshin, G. (2017)
612 Application of UV absorbance and fluorescence indicators to assess the formation of

biodegradable dissolved organic carbon and bromate during ozonation. Water Research 111, 154-162.

Aeschbacher, M., Graf, C., Schwarzenbach, R.P. and Sander, M. (2012) Antioxidant properties of humic substances. Environmental Science & Technology 46(9), 4916-4925.

Ramseier, M.K. and Gunten, U.v. (2009) Mechanisms of phenol ozonation—kinetics of formation of primary and secondary reaction products. Ozone: Science & Engineering 31(3), 201-215.

Bortolomeazzi, R., Sebastianutto, N., Toniolo, R. and Pizzariello, A. (2007) Comparative evaluation of the antioxidant capacity of smoke flavouring phenols by crocin bleaching inhibition, DPPH radical scavenging and oxidation potential. Food Chemistry 100(4), 1481-1489.

Wenk, J., Aeschbacher, M., Salhi, E., Canonica, S., von Gunten, U. and Sander, M. (2013) Chemical Oxidation of Dissolved Organic Matter by Chlorine Dioxide, Chlorine, And Ozone: Effects on Its Optical and Antioxidant Properties. Environmental Science & Technology 47(19), 11147-11156.

Chen, J., Gu, B., LeBoeuf, E.J., Pan, H. and Dai, S. (2002) Spectroscopic characterization of the structural and functional properties of natural organic matter fractions. Chemosphere 48(1), 59-68.

Anipsitakis, G.P., Dionysiou, D.D. and Gonzalez, M.A. (2006) Cobalt-Mediated Activation of Peroxymonosulfate and Sulfate Radical Attack on Phenolic Compounds. Implications of Chloride Ions. Environmental Science & Technology 40(3), 1000-1007.

Figure captions

Fig. 1. UVA_{254} decrease of different DOM fractions in Co(II)/PMS system as a function of time. Conditions: $[PMS]_0$ = 1.0 mM; Co(II) = 1.0 μM; DOM = 3.90 ± 0.11 mgC/L; pH = 8.00 ± 0.05 (10 mM borate buffer); T = 20°C.

Fig. 2. Correlation between *p*CBA decay and PMS exposure in Co(II)/PMS system with different DOM fractions. Conditions: $[PMS]_0$ = 1.00 mM; Co(II) = 1.00 μM; $[pCBA]_0$ = 1.00 μM; DOM = 3.90 ± 0.11 mgC/L; pH = 8.00 ± 0.05 (10 mM borate buffer); T = 20°C.

Fig. 3. Correlation between $CDOM_{fast}$ decrease and PMS exposure in Co(II)/PMS system. Conditions: $[PMS]_0$ = 1.00 mM; Co(II) = 1.00 μM; $[pCBA]_0$ = 1.00 μM; DOM = 3.90 ± 0.11 mgC/L; pH = 8.00 ± 0.05(10 mM borate buffer); T = 20°C.

Fig. 4. Correlation between normalized UVA_{254} and EDC decrease of different DOM fractions in Co(II)/PMS system. Conditions: PMS exposure = 0.00–8.04 M·s; Co(II) = 1.00 μM; DOM = 3.90 ± 0.11 mgC/L; pH = 8.00 ± 0.05 (10 mM borate buffer); T = 20°C. Areas a_0, a_1, and b illustrated the results obtained with a PMS exposure lower than 0.01, lower than 0.1, and larger than 0.1 M·s, respectively. R_E and R_U represented the normalized removal efficiency in EDC and UVA_{254}.

Fig. 5. TOC removal as a function of UVA_{254} decrease. Conditions: PMS exposure = 0.00–8.04 M·s; Co(II) = 1.00 μM; DOM = 3.90 ± 0.11 mgC/L; pH = 8.00 ± 0.05 (10 mM borate buffer); T = 20°C. Red dashed line was drawn to differentiate the correlation between $CDOM_{fast}$ and $CDOM_{slow}$ with TOC removal.

Fig. 6. Normalized emission spectra by its respective maximum fluorescence intensity of (a) S-HPOA, (b) B-HPOA, (d) R-HPO, and (d) C-HPO at an excitation wavelength of 230nm. The legend in each figure represented various PMS exposures.

Fig. 7. Proposed pathway of sulfate radical-induced DOM transformation

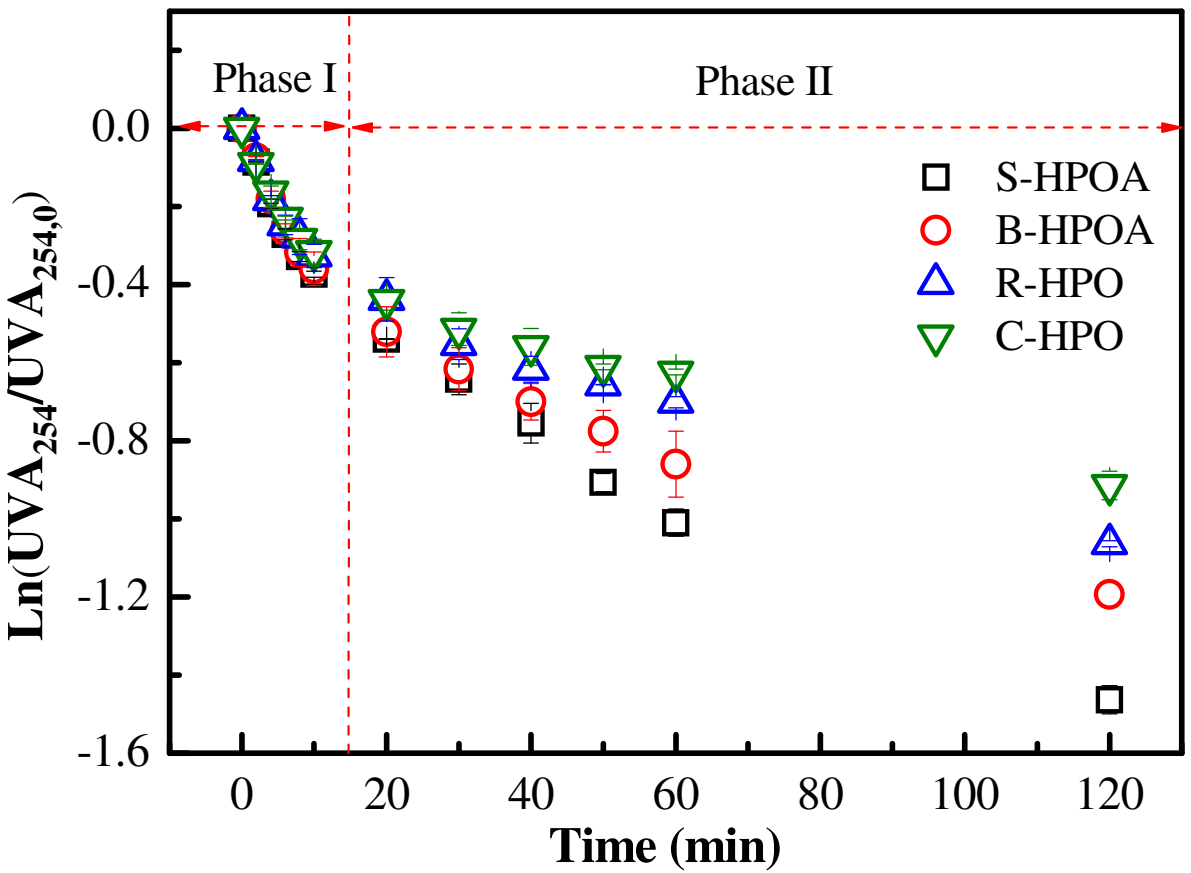

Fig. 1. UVA_{254} decrease of different DOM fractions in Co(II)/PMS system as a function of time. Conditions: $[PMS]_0$ = 1.0 mM; $Co(II)$ = 1.0 μM; DOM = 3.90 ± 0.11 mgC/L; pH = 8.00 ± 0.05 (10 mM borate buffer); T = 20°C.

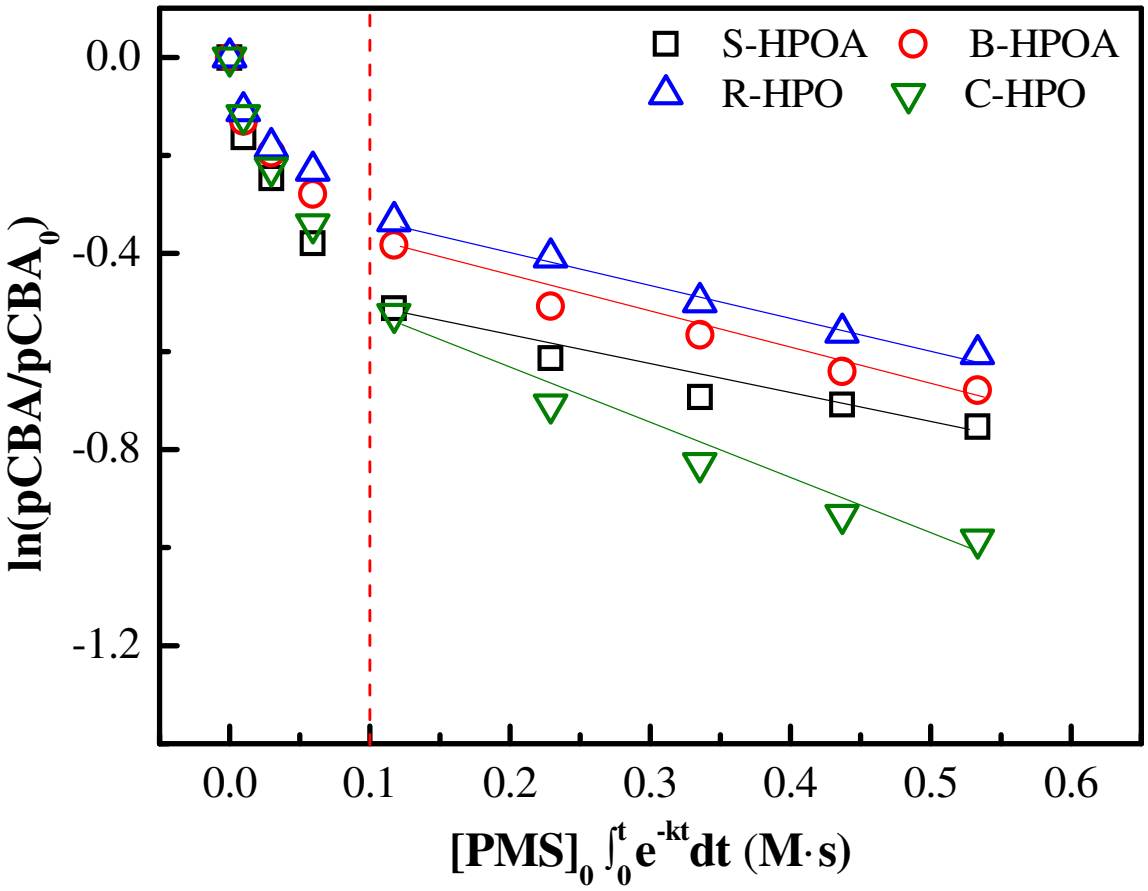

Fig. 2. Correlation between *p*CBA decay and PMS exposure in Co(II)/PMS system with different DOM fractions. Conditions: $[PMS]_0$ = 1.00 mM; $Co(II)$ = 1.00 μM; $[pCBA]_0$ = 1.00 μM; DOM = 3.90 ± 0.11 mgC/L; pH = 8.00 ± 0.05 (10 mM borate buffer); T = 20°C.

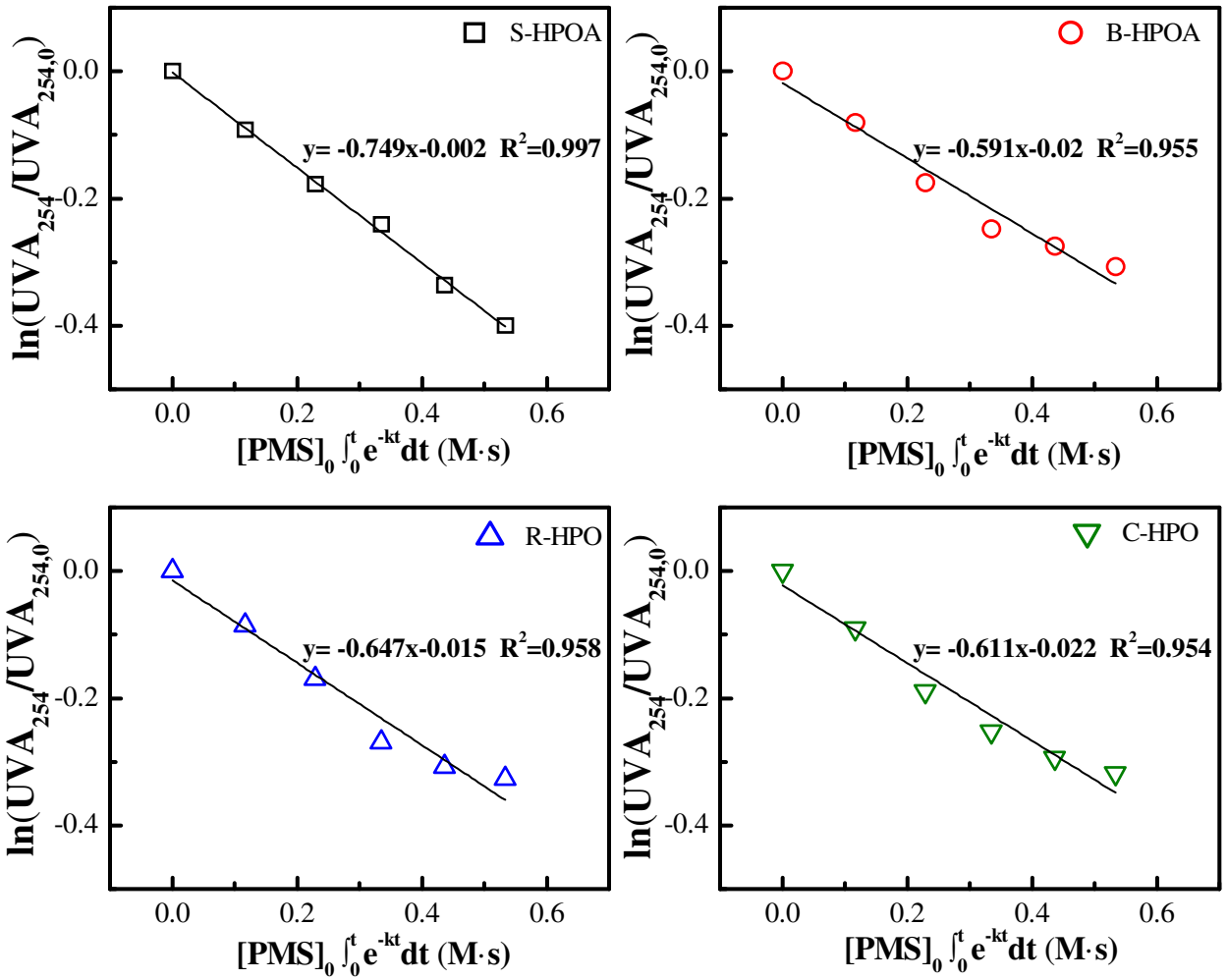

Fig. 3. Correlation between $CDOM_{fast}$ decrease and PMS exposure in Co(II)/PMS system. Conditions: $[PMS]_0$ = 1.00 mM; Co(II) = 1.00 μM; $[pCBA]_0$ = 1.00 μM; DOM = 3.90 ± 0.11 mgC/L; pH = 8.00 ± 0.05(10 mM borate buffer); T = 20°C.

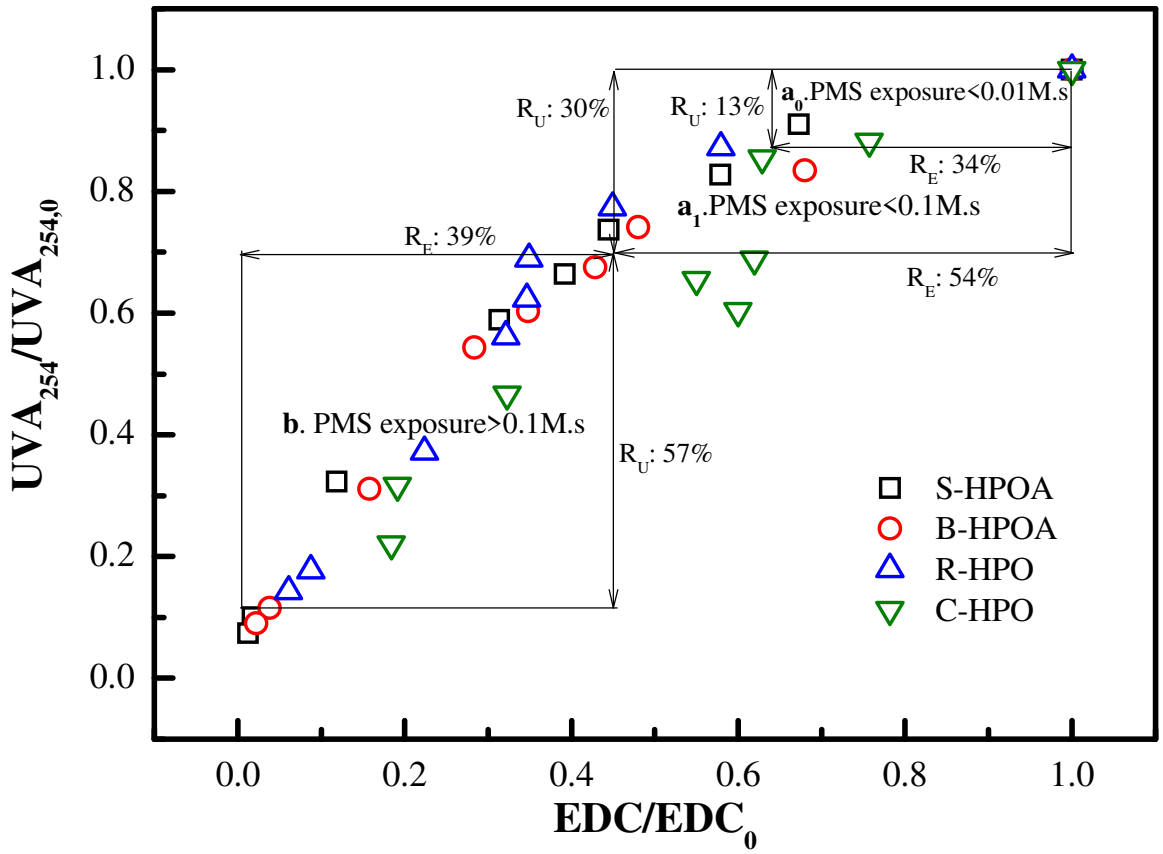

Fig. 4. Correlation between normalized UVA_{254} and EDC decrease of different DOM fractions in Co(II)/PMS reaction system. Conditions: PMS exposure = 0.00–8.04 M·s; Co(II) = 1.00 μM; DOM = 3.90 ± 0.11 mgC/L; pH = 8.00 ± 0.05 (10 mM borate buffer); T = 20°C. Areas a_0, a_1, and b illustrated the results obtained with a PMS exposure lower than 0.01, lower than 0.1, and larger than 0.1 M·s, respectively. R_E and R_U represented the normalized removal efficiency in EDC and UVA_{254}.

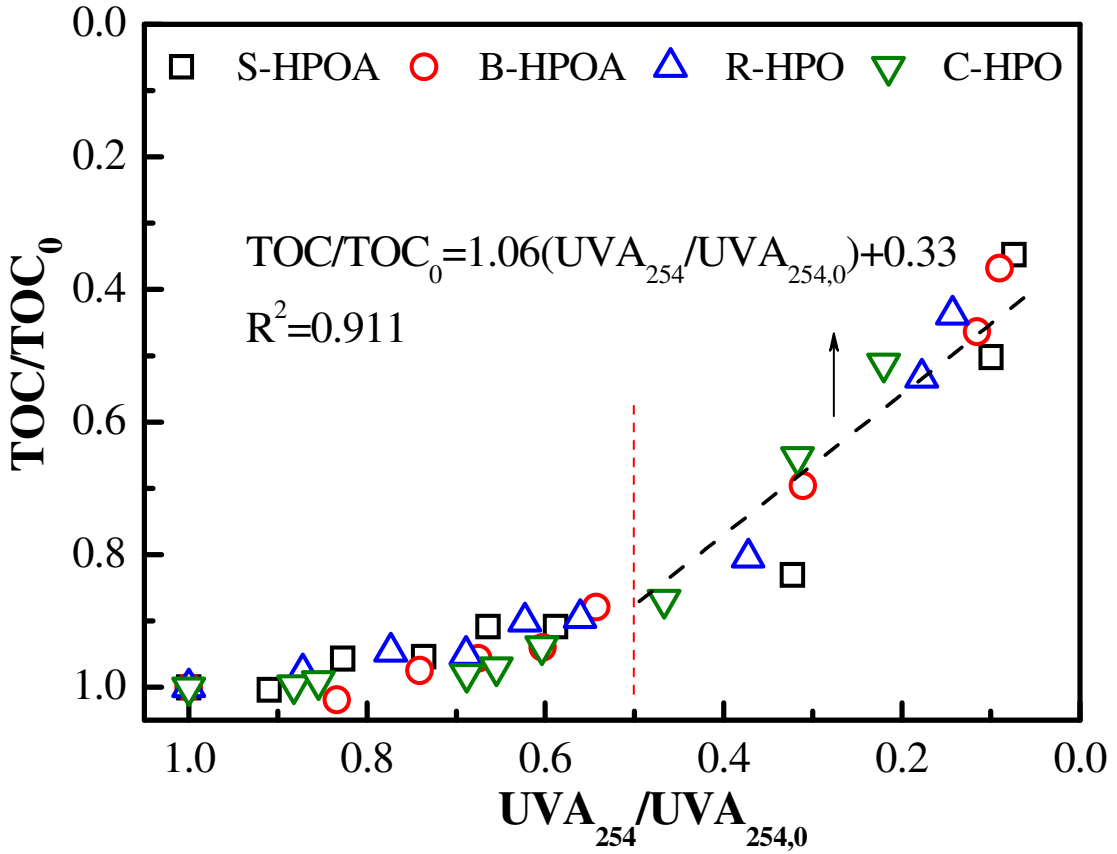

Fig. 5. TOC removal as a function of UVA_{254} decrease. Conditions: PMS exposure = 0.00–8.04 M·s; $Co(II)$ = 1.00 μM; DOM = 3.90 ± 0.11 mgC/L; pH = 8.00 ± 0.05 (10 mM borate buffer); T = 20°C. Red dashed line was drawn to differentiate the correlation between $CDOM_{fast}$ and $CDOM_{slow}$ with TOC removal.

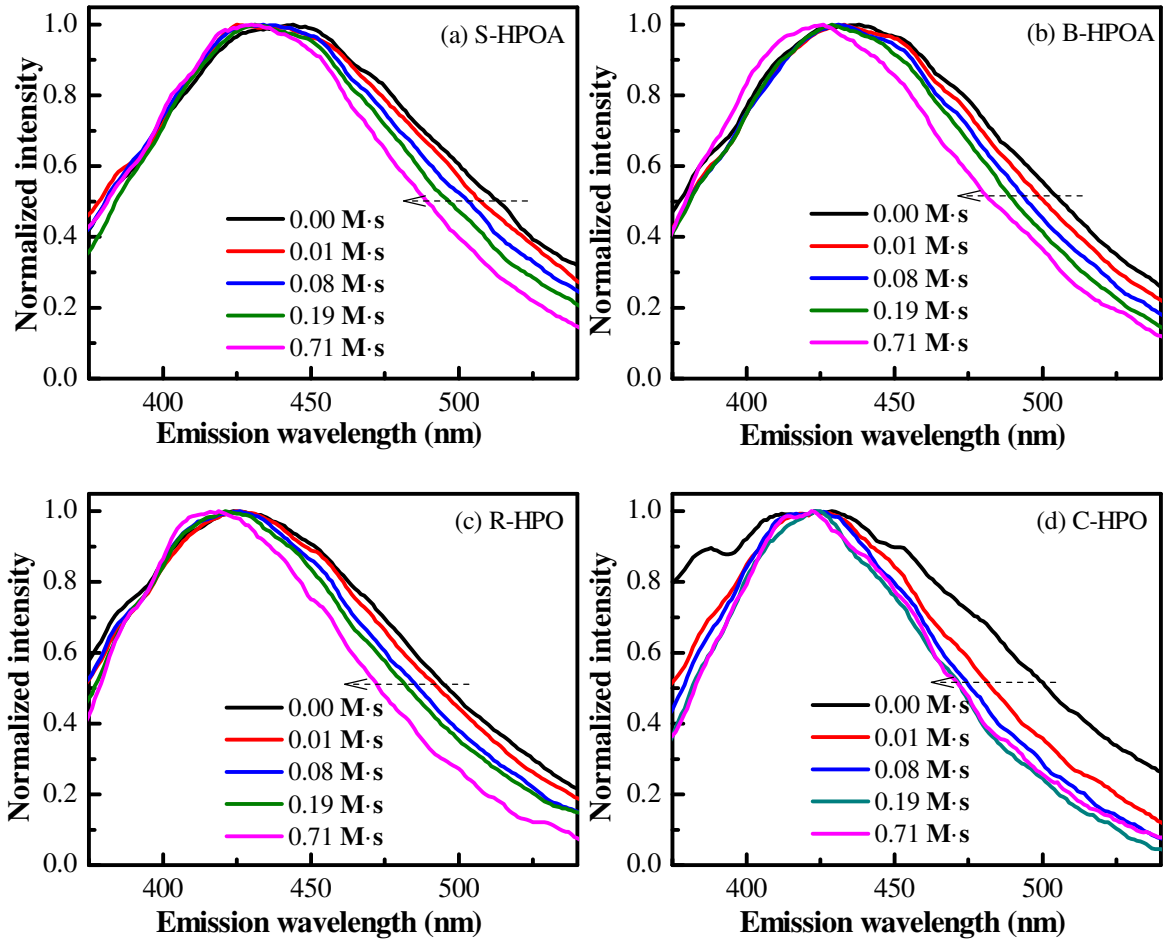

Fig. 6. Normalized emission spectra by its respective maximum fluorescence intensity of (a) S-HPOA, (b) B-HPOA, (d) R-HPO, and (d) C-HPO at an excitation wavelength of 230nm. The legend in each figure represented various PMS exposures.

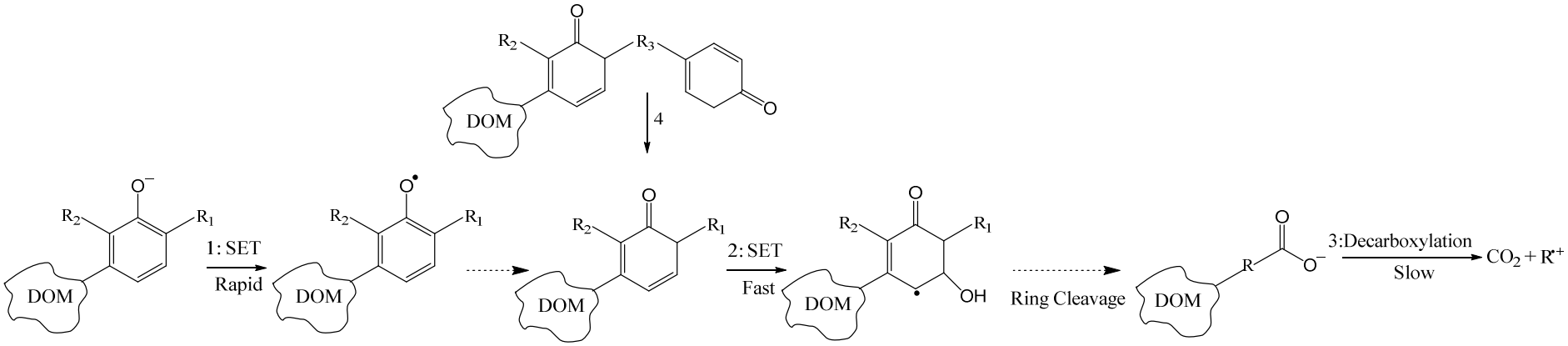

Fig. 7. Proposed pathway of sulfate radical-induced DOM transformation

Table 1. R_{ct} values in different DOM-containing systems under PMS exposure higher than 0.1 M·s ($ln(pCBA/pCBA_0) = -A([PMS]_0\int_0^t e^{-kt}dt) + B,\ R^2; R_{ct} = A/k_{SO_4^{\bullet-},pCBA}$)

DOM fraction	**A**	**R_{ct}**	**R^2**
S-HPOA	0.588	1.55×10^{-9}	0.935
B-HPOA	0.701	1.95×10^{-9}	0.970
R-HPO	0.670	1.86×10^{-9}	0.990
C-HPO	1.107	3.08×10^{-9}	0.968

Suwannee River, USA
SUVA: 4.78

Beaufort Reservoir, France
SUVA: 4.06

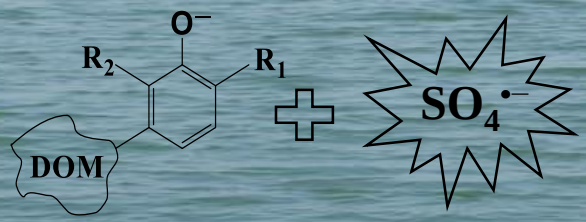

Ribou Reservoir, France
SUVA: 3.22

Colorado River, USA
SUVA: 2.14

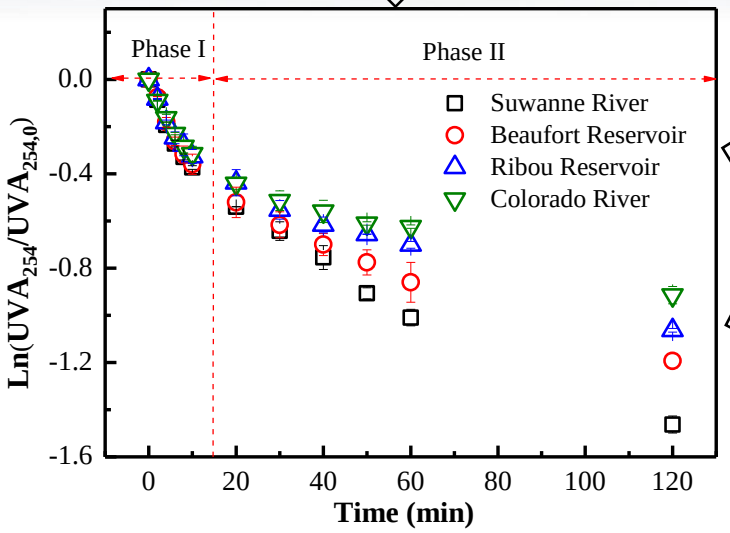

Phase I: $CDOM_{fast}$

$k_{CDOM\ fast, SO_4^{\bullet -}} :\sim 10^8\ M^{-1}s^{-1}$

Phase II: $CDOM_{slow}$

Carbon removal